SUPPLEMENTARY MATERIAL

Site description and sampling

The Ferris Coal at Wood Mountain Creek (49°25'20"N 106°19'50"W) and Rock Creek West (49°02'20"N 106°34'00") has been shown to span the K-Pg boundary, based on the distinctive 1–2 cm thick pink- to buff-coloured Ir-enriched claystone contained in each section (Nichols et al. 1986; Sweet and Braman 1992). The claystone is also coincident with a palynologically defined extinction of Cretaceous flora (Sweet and Braman 1992). At the time of the K-Pg boundary, the sites were (1) peat mires accumulating in the foreland basin of the ancestral Rocky Mountains (Jerrett et al. 2015); (2) inland, approximately equidistant between the shorelines of the (proto) Gulf of Mexico and the Boreal Sea (now the Arctic Ocean; Fig. 1); (3) at a palaeolatitude of approximately 54–56°N (van Hinsbergen et al. 2015); and (4) at negligible altitude, as evidenced by the persistence of marine conditions in the Maastrichtian Bearpaw Formation some tens of metres below the K-Pg boundary (Sweet and Braman, 2001). Vitrinite reflectance data (R_o) values for the Ferris Coal at the sites are <0.38%, indicating lignite rank (Bustin 1991), and ensuring the preservation of GDGTs (Schouten et al. 2004; 2013).

At both sites, the entire coal seam was contiguously sampled. Wood Mountain Creek was sampled in 2011 (56 samples). Sampling methodology and $\delta^{13}C_{org}$ analyses were previously published in Jerrett et al. (2015) and the latter are re-reported in Supplementary Table S1. Remaining material from the Wood Mountain Creek site were used for brGDGT analysis in this study. Rock Creek West was sampled in 2019 (36 samples), using the same methods as described in Jerrett et al. (2015).

Geochemical analysis and brGDGT method validation

All samples were freeze-dried and finely ground using a granite pestle and mortar prior to geochemical analyses.

Wood Mountain Creek

Approximately 0.5 g of sediment was solvent-extracted using ~20mL of DCM/methanol (9:1, v/v) in a Milestone Ethos Ex microwave extraction system at the Organic Geochemistry Unit (OGU) at the University of Bristol. Temperature in the microwave was programmed to increase linearly from room temperature to 70°C over 10 min at which it was held for 10 min, and then cooled to room temperature over 20 minutes. The total lipid extract (TLE) was dissolved in hexane:propanol (99:1, v/v) and filtered (0.45 μm PTFE) prior to analysis.

Samples were analysed for their GDGT content by high-performance liquid chromatography/atmospheric pressure chemical ionization–mass spectrometry (HPLC/APCI-MS) at the University of Bristol using a ThermoFisher Scientific Accela Quantum Access. Normal-phase separation was achieved following the method of Naafs et al. (2017a), which includes using two UHPL-LC silica columns for compound separation. Selective ion monitoring (SIM) was used to detect the [M+H]$^+$ ions of the following masses: *m/z* 1292, 1050, 1048, 1046, 1036, 1034, 1032, 1022, 1020, 1018, 744). The average standard deviation for duplicate MBT' measurements of an in-house standard was 0.026 units. The data are reported in Supplementary Table S1. The MBT'5Me index was calculated following De Jonge et al. (2014):

$$\text{MBT}'5\text{Me} = \frac{[\text{Ia}] + [\text{Ib}] + [\text{Ic}]}{[\text{Ia}] + [\text{Ib}] + [\text{Ic}] + [\text{IIa}] + [\text{IIb}] + [\text{IIc}] + [\text{IIIa}]}$$

The peat specific calibration (MAAT$_{peat}$, Naafs et al. 2017a) was used to convert MBT'5Me values into mean annual air temperatures:

$$\text{MAAT}_{peat} \ (°C) = 52.18(\text{MBT}'5\text{Me}) - 23.05$$

The CBT$_{peat}$ index was calculated following De Jonge et al. (2014):

$$CBT_{peat} = \log\frac{Ib + IIa' + IIb + IIb' + IIIa'}{Ia + IIa + IIIa}$$

The CBT$_{peat}$ values were converted into pH following Naafs et al. (2017a):

$$\text{pH} = 2.29(\text{CBT}_{peat}) + 8.07$$

Rock Creek West

For $\delta^{13}C_{org}$ analysis, samples were oven dried (30°C, 24 h), and decarbonated using hydrochloric acid (10% v/v) until any visible reaction had ceased. The samples were then repeatedly washed with deionised water until a neutral solution was obtained, and oven dried again (30°C, 24 h). Carbon isotope analyses were conducted at the University of Plymouth using a Thermo Scientific Delta V Advantage. Carbon-isotope ratios are expressed using the internationally accepted per mil (‰) standard notation relative to the Vienna Peedee belemnite (VPDB) standard (Table S1). Instrument calibration was achieved using three international standards: USGS 40 (l-glutamic acid, $\delta^{13}C$ = -26.389‰), USGS 24 (graphite, $\delta^{13}C$ = -16.049‰), and IAEA CH-7 (polyethylene, $\delta^{13}C$ = -32.151‰). The standard deviation on replicates in run analyses of the USGS 40 standard was ±0.12‰.

Approximately 1 g of sediment was solvent-extracted using 20mL of DCM/methanol (9:1, v/v) in a microwave assisted reactor system (MARS 6, CEM) at the University of Manchester following the same protocol as for Wood Mountain Creek. The TLE was separated into polar and apolar fractions by column chromatography, using hexane/DCM (9:1, v/v) and DCM/methanol (1:1, v/v) respectively as the eluents, and Al$_2$O$_3$ as the stationary phase. The polar fraction was re-dissolved in hexane/propanol (99:1, v/v) and filtered using a 0.45 µm PTFE filter prior to analysis.

Analysis of GDGTs was carried out using a Dionex LPG-U3400(SDN) UHPLC liquid chromatography system and Thermo Scientific Q Exactive Focus mass spectrometer with Atmospheric Pressure Chemical Ionisation (APCI) at the University of Plymouth. For the determination of MBT'5Me, the method of Hopmans et al. (2016) was adapted to this high-performance instrument employing a single Waters Acquity UPLC, BEH HILIC 1.7 µm (150 x 2.1 mm, 1.7 µm) column and precolumn at 40°C. Using solvents A (hexane) and B (9:1 hexane:isopropanol v/v) and a flow of 600 µl min -1, the mix started at 5% B (isocratic from 0–3 min), rising to 18 % B at 5 min (isocratic 5–10 min), rising to 35% B at 15 min and 100% B at 17.4 min, with 2.6 min re-equilibration time, which slightly shortened the analysis time. APCI was carried out in positive polarisation mode, at a capillary temperature of 275°C. Masses were scanned from *m/z* 200 to 2000, and resolved to 70,000 at *m/z* 200, with mass calibration carried out externally in electro spray ionisation mode, using auto-calibration Pierce LTQ Velos ESI positive ion calibration solution (n-butylamine, caffeine, MRFA, and Ultramark 1621). GDGTs were identified based on retention times and accurate masses: using 1022.00967 (brGDGT-Ia), 1019.99402 (brGDGT-Ib), 1017.97837 (brGDGT-Ic), 1036.02532 (brGDGT-IIa+IIa'), 1034.00967 (brGDGT-IIb+IIb'), 1031.99402 (brGDGT-

IIc+IIc'), 1050.04097 (brGDGT-IIIa+IIIa'), 1048.02532 (brGDGT-IIIb+IIIb'), 1046.00967 (brGDGT-IIIc+IIIc'), and 1292.24442 (crenarchaeol). Integration was carried out using Xcalibur 4.2 using QuanBrowser integration and data management. The data are reported in Supplementary Table S1. Temperature and pH were calculated using the same equations as for Wood Mountain Creek.

Comparison of HPLC data from University of Bristol and Plymouth University

To allow comparability between the samples analysed at the University of Bristol and the University of Plymouth, in particular for 6-Me separation, a set of standards and unrelated, representative samples, were analyzed at Bristol and Plymouth (marine standard and EH-8, Lengger et al. 2018). Further, as the HPLC-APCI-MS method for GDGT analyses was shortened to allow higher sample-throughput, taking advantage of the UHPLC-Orbitrap-MS system at the University of Plymouth, a subset of standards and samples were run on both methods ('long' for standard method acc. to Hopmans et al. (2016), 'short' method for 20 min method: shown are marine standard and EH-8 as described in Lengger et al. (2018); RCW-26 this work), to determine reproducibility (Fig. S1). The 'short' method is a variation of Hopmans et al. (2016), modified to run on one HPLC column (not two), and completes a sample run in 20 minutes (described in Vickers et al. 2020). As a result, the resolution is slightly compromised when compared to Hopmans et al. (2016), though the resolution of the 'short' method is comparable to the method at the University of Bristol (Fig. S1). The results from both 'short' and 'long' methods are very similar, with similar MBT' and MBT'5Me values calculated for both (Table S2). In addition, the 'long' method was also implemented at Plymouth and used for cross-calibration.

Fidelity of the MAAT record

Where possible, all GDGT analyses were duplicated (Table S1). A minority either could not be analysed a second time or showed a standard deviation >1 due to the low concentration of brGDGTs, and these samples and were eliminated from the study (Table S1). Shale samples were also excluded as the peat-specific calibration is not tested in shales. We note that the proxy is at or close to saturation (MBT'$_{5me}$ = 1) in a small number of retained datapoints.

To explore the fidelity of our GDGT-reconstructed temperatures, we examined the distributions of other GDGTs and biomarkers indicative of depositional environment. Previous work has shown that major changes in depositional setting, as inferred from reconstructed pH, can bias temperature estimates (Weijers et al. 2011; Inglis et al. 2019). Chen et al. (2022) and Halamka et al. (2022) showed that in the Acidobacterium Solibacter usitatus, the only organism known to produce a suite of brGDGTs comparable to that seen in the environment, the degree of methylation (captured in the MBT'5Me index) is correlated to MAAT but the degree of cyclisation (captured in the CBT' and CBTpeat indices) is not correlated to pH. This finding prompted the former to suggest that the degree of cyclisation-pH relationship is based on changes in community structure rather a physiological response; if so, that change in community structure could also affect the MBT'5Me-MAAT relationship, accounting for previous observations (De Jonge et al. 2021). Subsequent work (Rao et al., 2022) further suggests that changes in water depth in wetlands could also affect the MBT'5Me-MAAT relationship.

In the studied sections, CBT$_{peat}$-pH does vary (from 4.4 to 6.8; Table S1), though at neither Rock Creek West nor Wood Mountain Creek do these variations correlate with temperature changes. At Rock Creek West there is a decline in pH from 7 to 6.5 from the basal (Cretaceous) parts to the lowermost (Paleogene) parts of the coals, and thereafter pH varies between 5 and 6. At Wood Mountain Creek, the pH is highly variable in the Cretaceous (from 4.4 to 6.3), but in the earliest Paleogene declines from 6.5, and thereafter varies between 5 and 6. The patterns are consistent with palynological (Sweet and Braman 1992) and petrographic (Sweet and Cameron 1991; Jerrett et al. 2015) data that imply that the coal at both sites represents a hydroseral succession upwards from (typically more alkaline) ponded, disconnected forested rheotrophic mires in-filling topographic hollows, to (typically more acidic) aerially expansive herbaceous, possibly ombrotrophic mires. We observe no correlation between pH and temperature, and there is no change in CBT associated with the post-boundary cooling. Although the variations in CBT-derived pH are larger than those observed in other lignite settings (e.g., Lauretano et al. 2021), they are smaller than the previous studies where pH was inferred to bias temperature estimates (Weijers et al. 2011; Inglis et al. 2019). Moreover, at Rock Creek West, the clear decline in post-boundary temperatures is associated with near-constant pH values. Some of the smaller variations in pH do coincide with changes in reconstructed temperature, however, and we therefore focus on the main trends in MAAT.

Further evidence for relatively stable environmental conditions comes from the BIT index (Hopmans et al. 2004), which reflects the relative abundance of brGDGTs to crenarchaeol, an isoGDGT produced by soil and aquatic Thaumarchaeota. BIT values are typically >0.99, again consistent with a persistent peatland setting, but in a few intervals values decline to 0.97 (Table S1). Zheng et al (2015) showed that intervals of severe peatland drying are associated with increases in the fractional abundance of crenarchaeol relative to isoGDGTs. Wood Mountain Creek appears to have experienced such episodes just above and below the KPg Boundary (Table S1); however, these do not coincide with temperature change. The isoGDGT:brGDGT ratio at Wood Mountain Creek is somewhat variable throughout and shows no relationship with temperature. Rock Creek West shows increased crenarchaeol abundance near the top of the section, coincident with an interval of greater isoGDGT:brGDGT ratios and the coolest temperatures recorded at this site. These changes suggest a relationship between cooling and apparent peatland drying but this speculation requires further investigation.

To further explore the wider biomarker distribution at these sites, we determined the bacterial hopane isomerisation ratio. Isomerisation at the C_{17} and C_{21} positions (from the 17▯,21▯(H) to the 17▯,21▯(H) configuration) normally occurs with increasing thermal maturity over millions of years (Mackenzie et al. 1980), but this process is accelerated, especially for the C_{31} hopane, under acidic conditions in wetlands. Recent work showed that the degree of isomerisation for the C_{31} hopane in wetlands provides an independent method to reconstruct pH (Inglis et al. 2018, 2019).

The apolar fractions were analysed using an Agilent 7890A gas chromatograph (GC) interfaced to an Agilent 5975C MSD mass spectrometer (MS) operated in electron ionisation scan/SIM mode (scanning range, m/z 50–600; SIM masses used: m/z 57, 66, 191 and 205; ionisation energy, 70 eV; solvent delay of 2.5 min) using helium as the carrier gas at a constant flow (1 mL/min). The GC was equipped with an Agilent 7683B auto-sampler and programmable temperature vaporization (PTV) inlet. The samples were dissolved in hexane prior to injection, injected using pulsed split-less injection (1 μL; inlet pressure of 25 psi for 0.75 min), and separated on a Zebron ZB-5MS capillary column (Phenomenex; length 30 m; 250 μm ID, 0.25 μm film thickness). The heated interface (MSD

transfer line) and PTV temperatures were set to 280°C, the mass source, at 230°C and the mass spectrometer quadrupole at 150°C. The samples were injected at 50°C and the oven was programmed to ramp to 130°C at 20°C/min and then to 310°C at 6°C/min, at which it was kept isothermally for 15 min. Compounds were identified by comparison of their mass fragments (m/z) with The National Institute of Standards and Technology (NIST) library. Quantitative data were determined by comparison of individual peak areas with a known concentration of the internal standard deuterated tetracosane, added prior to analyse and pH was calculated using the C_{31} hopanes following Inglis et al. (2018):

$$\text{pH} = 5.22 \left(C_{31} \ hopane \ \frac{\beta\beta}{\alpha\beta + \beta\beta} \right) + 3.11$$

Overall values of the C_{31} $\beta\beta$ /($\alpha\beta$ + $\beta\beta$) hopane ratio range between 0.06 and 0.42, translating in to pH values between 3.4 and 5.3. These values are lower compared to the brGDGT-based estimates, but consistent with an acidic peat forming environment.

Another unusual feature of the brGDGT distribution of these sections is the lack of 6'-methyl brGDGTs in nearly all samples despite reconstructed pH between 7 and 4. At such pH and especially above pH 6, 6'-methyl brGDGTs do occur in modern mineral soils and peatlands (Naafs et al. 2017a, 2017b). This is not an artefact of the analytical method, as we cross-checked with the "long" method in Plymouth (Fig. S1). Therefore, we interpret our MAAT record cautiously, focusing primarily on the most pronounced variations which are not correlated with changes in CBT. That is, peak temperatures immediately above the K-Pg boundary, and the long-term decline in MAATs in the Paleogene part of the record.

Age Model

Correlation: First order correlation between the two sites is based on the occurrence of the distinctive Ir-bearing claystone that is also palynologically enriched in fern spores (Sweet and Braman, 1992), and marks the base of the Paleogene. Its base is used as a horizontal datum in Figure 2 and Figure S2. Jerrett et al. (2015) interpreted these coals to represent, at least in part, small, disconnected rheotrophic mires, readily subject to local autogenic clastic input. Consequently, a lithostratigraphic approach would not be appropriate for the generation of other chronostratigraphic tie-points in this case. Instead, secondary tiepoints are provided by inflexion points on their respective $\delta^{13}C_{org}$ stratigraphies of the two sites (Tiepoints 1–9; Figs. 2 and S2). These can be interpreted as representing a more regional stratigraphic signal relating to changes in the carbon isotopic composition of the atmosphere the plants in the peats were metabolising (Arens and Jahren, 2000). This correlation is consistent with an independent correlation between the two sites based on petrographic criteria by Jerrett et al. (2015).

Timescales: Estimations of the duration of time represented by such short stratigraphies are difficult. Broad estimates of the duration of time represented by the two coal seams, however, can be estimated from the absolute age determinations of Renne et al. (2013) at the coal-bearing K-Pg site at Hell Creek Marina Road (Montana), located 170 km SSW of Rock Creek West (Fig. 1). The stratigraphy of the site is represented by 160 cm of coal, which directly overlies the Ir-enriched claystone marking the K-Pg boundary. The coal contains two tuffs termed Z2 and Z1, 80 cm and 120 cm above the K-Pg boundary, respectively. $^{40}Ar/^{39}Ar$ dating of sanidines in the tuffs yield an age of 66.019 ±0.021 Ma for Z2, and 66.003 ±0.033 Ma for Z1 (Renne et al. 2013), giving a most likely

duration of 16 ka for the 40 cm of intervening coal (i.e., 1 m represents 40 ka). Error estimates of the ages suggest a maximum possible duration of 90 ka is possible for the 40 cm of intervening coal (i.e., 1 m represents 175 ka), and an unlikely minimum duration that equates to instantaneous deposition. Compilations of Holocene peat accumulation rates show that long-term, time averaged peat accumulation rates decrease by half an order of magnitude from Tropics to high latitudes (Diessel et al. 2000). We consider the distance between Hell Creek Road, whence we derive our peat accumulation rates, and our Saskatchewan sites to represent negligible latitudinal difference. It therefore provides the best, and a realistic age model for our sites, in the absence of such radiometric data at the study locations.

In Supplementary Table S3, the most likely (1 m = 40 ka), minimum (1 m = 0 ka), and maximum (1 m = 175 ka) duration of time represented by the coal is used to date Tiepoints 1–9, relative to the K-Pg boundary (Fig. 2 and S3). Differences in thicknesses of coal between the tiepoints (i.e., differences in thicknesses of the $\delta^{13}C_{org}$ excursion stratigraphies) at Rock Creek West and Wood Mountain Creek (Fig. 2 and S2) clearly imply that there were differences in synchronous peat accumulation rates and/or post-depositional compaction of the peat at the two sites (and also between these sites and the Hell Creek Marina Road site of Renne et al. 2013). These differences highlight uncertainties, but the approach places clear absolute errors in the timescales of MAAT change interpreted in this study. The ages relative to the K-Pg boundary that we use for Tiepoints 1–9 are based on the average determined for Rock Creek West, and Wood Mountain Creek (Table S3).

Having established the best-estimate ages of Tiepoints 1–9 (Table S3), the midpoint of each sample was linearly extrapolated between the ages of the Tiepoints to ascribe each an individual age relative to the K-Pg boundary (Table S4). MAAT for each datapoint were plotted against these ages to make Figure 3.

FIGURE AND TABLE CAPTIONS

Figure S1. *Chromatograms showing the difference in resolution of individual brGDGTs and their isomers in the 'Long' method at Plymouth University (A), the 'Short' method at Plymouth University (B), and the 'Long' method at University of Bristol. 6-methyl-GDGTs are indicated with '.*

Figure S2. *$\delta^{13}C_{org}$ (blue), brGDGT mean annual air temperature (MAAT; purple), CBT_{peat}-pH (red) records from Wood Mountain Creek and Rock Creek West, Saskatchewan, plotted against height relative to the K-Pg boundary. Vertical error bars show the stratigraphic range of each sample. Dashed lines show chemostratigraphic ($\delta^{13}C_{org}$) correlation tiepoints. Solid line shows the Ir-claystone K-Pg datum. On the lithology log, Co = coal, ShC = shaley coal, CSh = coaly shale, Sh = shale, and Ir = iridium-enriched claystone.*

Table S1. *Stratigraphic and lithological data, GDGT abundances, proxy calculations (MBT'5Me, MAAT, CBT_{peat}, pH, and hopane ratio), and $\delta^{13}C_{org}$ for all samples reported in this study. MBT'5Me (Columns AH, BJ, BQ) calculated from De Jonge et al. (2015). MAAT (Columns AI, BK, BR) calculated from Naafs et al. (2017a). CBT_{peat} (Columns AJ, BL, BT) calculated from Naafs et al. (2018). pH (Columns AK, BM, BU) calculated from Naafs et al. (2018). Hopane ratio (Column BV) calculated from Inglis et al. (2018). Blank cells (columns J–AC, AL–BE) denote below the detection limit/unquantifiable GDGTs. The $\delta^{13}C_{org}$ values (columns BX–CE) for Wood Mountain Creek are from Jerrett et al. (2015). All other data was generated for this study. Where the standard deviation of MAAT > 1, this sample*

was omitted from the study. Where polar fraction analysis not undertaken or duplicated, this sample was omitted from the study.

Table S2. *Comparison of MBT, MBT'5Me proxy values calculated from the 'Short' and 'Long' HPLC-APCI-MS methods at Plymouth University and the 'long' method at the University of Bristol. (std= standard, RCW= Rock Creek West, SD= standard deviation).*

Table S3. *Age of Tiepoints 1–9 (Fig. S2) at Rock Creek West and Wood Mountain Creek relative to the K-Pg boundary (columns C–E and G–I respectively), applying the minimum (1 m = 0 ka), most likely (1 m = 40 ka), and maximum (1 m = 175 ka) duration of time represented by the coal from Renne et al. (2013). Also shown are the average relative ages of the tiepoints from Rock Creek West and Wood Mountain Creek (columns L-N). The most likely duration of the average tiepoint ages (column M) are the values used to generate the ages for each datapoint in Supplementary Table S4.*

Table S4. *All samples, and their assigned ages generated through linear interpolation of the position of their midpoint between tiepoints. The ages of the tiepoints are from column M (Supplementary Table S3). Also shown are the MAAT (°C) and mean $\delta^{13}C$ (‰) values from Supplementary Table S1. These data are used to plot Figure 3.*

Table S5. *Statistical analysis of MAAT data. MAAT data were separated into four temporal bins: pre-K-Pg boundary (-5–0 ka), 0–10 ka, 10–20 ka, and 20–30 ka. These bins were then analysed using two-sample, equal variances t-tests to determine the statistical significance of temperature trends. These data are included in Figure 3.*

Supplementary references

Arens, N.C., Jahren, A.H., and Amundson, R., 2000, Can C3 plants faithfully record the isotopic composition of atmospheric carbon dioxide?: Paleobiology, v. 26, p. 137–164, doi: 10.1666/0094-8373(2000)026<0137:CCPFRT>2.0.CO;2.

Bustin, R. M., 1991, Organic maturity in the western Canada sedimentary basin: International Journal of Coal Geology, v. 19, p. 319-358, doi: 10.1016/0166-5162(91)90026-F.

De Jonge, C., Kuramae, E. E., Radujković, D., Weedon, J. T., Janssens, I. A., and Peterse, F., 2021, The influence of soil chemistry on branched tetraether lipids in mid-and high latitude soils: Implications for brGDGT-based paleothermometry: Geochimica et Cosmochimica Acta, v. 310, p. 95-112, doi: 10.1016/j.gca.2021.06.037.

Diessel, C., Boyd, R., Wadsworth, J., Leckie, D., and Chalmers, G., 2000, On balanced and unbalanced accommodation/peat accumulation ratios in the Cretaceous coals from Gates Formation, Western Canada, and their sequence-stratigraphic significance: International Journal of Coal Geology, v. 43, p. 143-186, doi: 10.1016/S0166-5162(99)00058-0.

Hopmans, E. C., Weijers, J. W., Schefuß, E., Herfort, L., Damsté, J. S. S., and Schouten, S., 2004, A novel proxy for terrestrial organic matter in sediments based on branched and isoprenoid tetraether lipids: Earth and Planetary Science Letters, v. 224, p. 107-116, doi: 10.1016/j.epsl.2004.05.012.

Hopmans, E. C., Schouten, S., and Damsté, J. S. S., 2016, The effect of improved chromatography on GDGT-based palaeoproxies: Organic Geochemistry, v. 93, p. 1-6, doi: 10.1016/j.orggeochem.2015.12.006.

Inglis, G. N., Farnsworth, A., Collinson, M. E., Carmichael, M. J., Naafs, B. D. A., Lunt, D. J., Valdes, P.J. and Pancost, R.D., 2019, Terrestrial environmental change across the onset of the PETM and the associated impact on biomarker proxies: A cautionary tale: Global and Planetary Change, v. 181, 102991, doi: 10.1016/j.gloplacha.2019.102991.

Inglis, G. N., Naafs, B. D. A., Zheng, Y., McClymont, E. L., Evershed, R. P., and Pancost, R. D., 2018, Distributions of geohopanoids in peat: Implications for the use of hopanoid-based proxies in natural archives: Geochimica et Cosmochimica Acta, v. 224, p. 249-261, doi: 10.1016/j.gca.2017.12.029.

Jerrett, R. M., Price, G. D., Grimes, S. T., Dawson, A. T., 2015, A paleoclimatic and paleoatmospheric record from peatlands accumulating during the Cretaceous-Paleogene boundary event, Western Interior Basin, Canada: Geological Society of America Bulletin, v. 127, p. 1564–1582; doi: 10.1130/B31166.1.

Lauretano, V., Kennedy-Asser, A. T., Korasidis, V. A., Wallace, M. W., Valdes, P. J., Lunt, D. J., Pancost, R.D., and Naafs, B. D. A., 2021, Eocene to Oligocene terrestrial Southern Hemisphere cooling caused by declining pCO2: Nature Geoscience, v. 14, p. 659-664, doi: 10.1038/s41561-021-00788-z.

Lengger, S. K., Sutton, P. A., Rowland, S. J., Hurley, S. J., Pearson, A., Naafs, B. D. A., Dang, X., Inglis, G.N., and Pancost, R. D., 2018, Archaeal and bacterial glycerol dialkyl glycerol tetraether (GDGT) lipids in environmental samples by high temperature-gas chromatography with flame ionisation and time-of-flight mass spectrometry detection: Organic Geochemistry, v. 121, p. 10-21, doi: 10.1016/j.orggeochem.2018.03.012.

Mackenzie, A.S., Patience, R.L., Maxwell, J.R., Vandenbroucke, M., Durand, B., 1980, Molecular parameters of maturation in the Toarcian shales, Paris Basin, France—I. Changes in the configurations of acyclic isoprenoid alkanes, steranes and triterpanes: Geochimica et Cosmochimica Acta, v. 44, p. 1709-1721, doi: 10.1016/0016-7037(80)90222-7.

Naafs, B.D.A., Inglis, G.N., Zheng, Y., Amesbury, M.J., Biester, H., Bindler, R., Blewett, J., Burrows, M.A., Del Castillo Torres, D., Chambers, F.M., et al., 2017a, Introducing global peat-specific temperature and pH calibrations based on brGDGT bacterial lipids: Geochimica et Cosmochimica Acta, v. 208, p. 285-301, doi: 10.1016/j.gca.2017.01.038.

Naafs, B.D.A., Gallego-Sala, A.V., Inglis, G.N., Pancost, R.D., 2017b. Refining the global branched glycerol dialkyl glycerol tetraether (brGDGT) soil temperature calibration. Organic Geochemistry, v. 106, p. 48-56, doi: 10.1016/j.orggeochem.2017.01.009.

Naafs, B. D. A., Rohrssen, M., Inglis, G. N., Lähteenoja, O., Feakins, S. J., Collinson, M. E., Kennedy, E.M., Singh, P.K., Singh, M.P., Lunt, D.J., et al., 2018, High temperatures in the terrestrial mid-latitudes during the early Palaeogene: Nature Geoscience, v. 11, p. 766-771, doi: 10.1038/s41561-018-0199-0.

Nichols, D. J., Jarzen, D. M., Orth, C. J., and Oliver, P. Q., 1986, Palynological and iridium anomalies at Cretaceous-Tertiary boundary, south-central Saskatchewan: Science, v. 231, p. 714-717, doi: 10.1126/science.231.4739.71.

Rao, Z., Guo, H., Wei, S., Cao, J., and Jia, G., 2022, Influence of water conditions on peat brGDGTs: A modern investigation and its paleoclimatic implications: Chemical Geology, v. 606, 120993, doi: 10.1016/j.chemgeo.2022.120993.

Renne, P. R., Deino, A. L., Hilgen, F. J., Kuiper, K. F., Mark, D. F., Mitchell III, W. S., Morgan, L.E., Mundil, R. and Smit, J., 2013, Time scales of critical events around the Cretaceous-Paleogene boundary: Science, v. 339, p. 684-687, doi: 10.1126/science.1230492.

Schouten, S., Hopmans, E.C., Sinninghe Damsté, J.S., 2004, The effect of maturity and depositional redox conditions on archaeal tetraether lipid palaeothermometry: Organic Geochemistry v. 35, p. 567-571, doi: 10.1016/j.orggeochem.2004.01.012.

Schouten, S., Hopmans, E.C., Sinninghe Damsté, J.S., 2013, The organic geochemistry of glycerol dialkyl glycerol tetraether lipids: A review: Organic Geochemistry, v. 54, p. 19-61, doi: 10.1016/j.orggeochem.2012.09.006.

Sweet, A. R., and Braman, D. R., 2001, Cretaceous–Tertiary palynofloral perturbations and extinctions within the *Aquilapollenites* Phytogeographic Province: Canadian Journal of Earth Sciences, v. 38, p. 249-269, doi: 10.1139/e00-024.

Sweet, A. R., and Cameron, A. R., 1991, Palynofacies, coal petrographic facies and depositional environments: Amphitheatre Formation (Eocene to Oligocene) and Ravenscrag Formation (Maastrichtian to Paleocene), Canada: International Journal of Coal Geology, v. 19, p. 121-144, doi: 10.1016/0166-5162(91)90017-D.

Sweet, A. R., and Braman, D. R., 1992, The KT boundary and contiguous strata in western Canada: interactions between paleoenvironments and palynological assemblages: Cretaceous Research, v. 13, p. 31-79, doi: 10.1016/0195-6671(92)90027-N.

van Hinsbergen, D. J., De Groot, L. V., van Schaik, S. J., Spakman, W., Bijl, P. K., Sluijs, A., Langereis, C.G., and Brinkhuis, H., 2015, A paleolatitude calculator for paleoclimate studies: PloS one, v. 10, e0126946, doi: 10.1371/journal.pone.0126946.

Vickers, M. L., Lengger, S. K., Bernasconi, S. M., Thibault, N., Schultz, B. P., Fernandez, A., Ullmann, C.V., McCormack, P., Bjerrum, C.J., Rasmussen, J.A., et al., 2020, Cold spells in the Nordic Seas during the early Eocene Greenhouse: Nature Communications, v. 11, p. 1-12, doi: 0.1038/s41467-020-18558-7.

Weijers, J. W., Schouten, S., van den Donker, J. C., Hopmans, E. C., and Damsté, J. S. S., 2007, Environmental controls on bacterial tetraether membrane lipid distribution in soils: Geochimica et Cosmochimica Acta, v. 71, p. 703-713, doi: 10.1016/j.gca.2006.10.003.

Zheng, Y., Li, Q., Wang, Z., Naafs, B. D. A., Yu, X., and Pancost, R. D., 2015, Peatland GDGT records of Holocene climatic and biogeochemical responses to the Asian Monsoon: Organic Geochemistry, v. 87, p. 86-95, doi: 10.1016/j.orggeochem.2015.07.012.
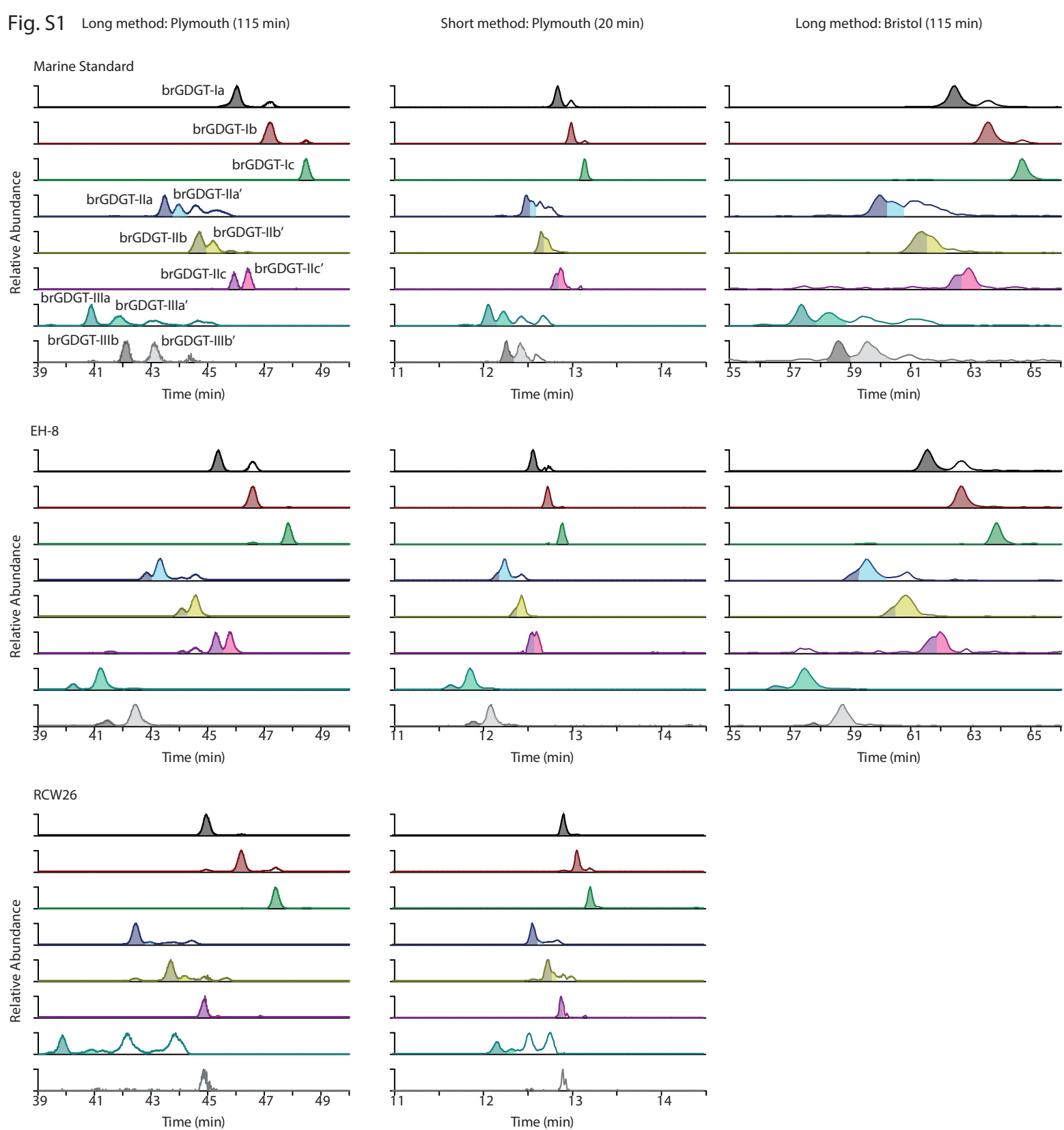
Fig. S1

Long method: Plymouth (115 min)   Short method: Plymouth (20 min)   Long method: Bristol (115 min)

Marine Standard

brGDGT-Ia
brGDGT-Ib
brGDGT-Ic
brGDGT-IIa   brGDGT-IIa'
brGDGT-IIb   brGDGT-IIb'
brGDGT-IIc   brGDGT-IIc'
brGDGT-IIIa   brGDGT-IIIa'
brGDGT-IIIb   brGDGT-IIIb'

EH-8

RCW26

Fig. S2